Electron-electron interactions in low-dimensional Si:P delta layers

Joseph A. Hagmann ⬤,[*] Xiqiao Wang, Ranjit Kashid, Pradeep Namboodiri, Jonathan Wyrick, Scott W. Schmucker,
M. D. Stewart, Jr. ⬤, Richard M. Silver, and Curt A. Richter

Physical Measurement Laboratory, National Institute for Standards and Technology, Gaithersburg, Maryland 20899, USA

Scientists have long studied the physics of highly disordered conducting systems, seeking to understand the multitude of quantum phenomena that govern how electrons move through material systems. Recently, research into silicon-based quantum computing has made disordered conducting systems, such as Si:P monolayers embedded in isotopically pure Si, technically relevant. Consequently, applying and advancing the theoretical frameworks developed to describe electron behavior in disordered systems is a necessary objective in this field of research. This study investigates key components of dopant-based Si quantum computing devices: embedded regions of highly doped delta layers (δ layers). We examine the transport behavior and the electron-electron interaction (EEI) physics in embedded Si:P δ layers by means of self-consistent magnetotransport measurements. Parameters associated with the electronic transport offer a meaningful quantitative characterization of δ-layer quality and dopant diffusion. In addition, by examining EEI behaviors in a set of samples with embedded Si:P δ layers produced with different PH_3 exposure procedures prior to Si encapsulation, we show how details of material synthesis affect the dimensionality of charge carrier interactions in embedded Si:P δ layers. The relationship between δ-layer confinement and EEI screening lengths is established here. This understanding will help validate important models used for device simulation and design and lead to improvements in the control of electrostatic gating of and tunneling transport through Si:P single atom transistors.

I. INTRODUCTION

Positioning phosphorus dopants on Si (100) surfaces with atomistic control by means of scanning tunneling microscope (STM) -based hydrogen lithography [1–4] is used to produce atomic-scale devices [5] such as wires [6,7], quantum dots [8,9], and single dopant transistors [10]. Furthermore, it is a promising metrological tool to study the building blocks of the Si-based Kane quantum computer [11–13] and the ultimate scaling of conventional semiconductor devices [14]. Researchers have addressed the challenge of producing high-quality epitaxially overgrown silicon to embed [15,16] and electrically activate phosphorus dopants [17] to form deterministically placed atomic-scale devices and metallic delta-layer (δ-layer) regions, which serve as the electrical gates, contacts, and interconnects. Control over this fabrication process has been improved by the development of several sample synthesis methods. For example, limiting the substrate temperature during encapsulating overgrowth to 250 °C has been shown to limit dopant diffusion and segregation of the incorporated phosphorus [18,19]. Beginning the encapsulation overgrowth by growing a locking layer of several monolayers of Si deposited at room temperature has been shown to further reduce the movement of itinerant dopants during Si overgrowth [20]. To this end, we have demonstrated, in previous work, a method for the accurate measurement of

phosphorus diffusion and segregation by means of a series of nondestructive, temperature-dependent, magnetotransport measurements. Analysis of measured sample magnetoresistivities at low temperatures reveals, with high resolution, the thickness of the electron gas hosted by an ultrathin embedded phosphorus δ layer in silicon [21]. This method, which involves the careful analysis of the weak localization signals in the magnetotransport data from measurements in perpendicular and parallel magnetic fields, offers a sensitive probe of δ-layer thickness that overcomes the resolution limitations of secondary ion mass spectroscopy (SIMS) [22,23].

The promising advances in the synthesis of embedded Si:P with good control of dopant placement and limited dopant movement during Si encapsulation open the door for the development of silicon-based single atom devices. However, in order to engineer Si:P single atom devices with good control of device behavior, researchers must understand the physics of the component materials. The study presented here investigates the nature of the conducting electrons in embedded high-dopant-density Si:P δ layers in terms of interaction distances and scattering geometries. We demonstrate an integrated approach to the measurement and analysis of electron-dephasing and electron-electron effects in very-low-mobility, highly disordered embedded two-dimensional (2D) systems. By magnetotransport investigation, we obtain parameters associated with quantum interference effects, measure the conducting layer thickness, and determine contributions to the Drude conductivity due to electron-electron interactions (EEIs)

_____
[*]Corresponding author: joseph.hagmann@nist.gov

and related parameters by using the well-known theoretical framework of Altshuler and Aronov [24]. We show how these methods reveal important transport physics in highly P-doped δ layers confined to nanometer-scale thicknesses embedded in Si—a material system of major relevance to Si-based quantum computing [5,12,13,25,26]. This approach can also be applied to other disordered 2D conducting materials (above their metal-insulator transitions) in the regime of diffusive transport, 2D localization, and 2D electron-electron scattering.

Methods similar to those presented here have been used by Kuntsevich *et al.* to study EEI in Si metal-oxide-semiconductor field-effect transistor (MOSFET) two-dimensional electron gases (2DEGs) in a magnetic field [27], and by Minkov *et al.* to study EEI in low-mobility GaAs-based 2DEG systems [28], showing the promise of these methods in measuring EEI effects in 2DEGs formed at insulator-insulator interfaces (e.g., inversion layers and quantum wells). However, it has not yet been shown that this approach can be applied to quantitatively extract EEI parameters from transport data for dimensionally confined, highly doped regions in an insulator with mobilities several orders of magnitude lower. We show that, at low temperatures—temperatures shown to sustain state coherence in Si qubits [25,26]—these effects can, indeed, be measured in well-confined, highly doped Si:P δ layers with very low mobilities. Moreover, we show that, at sufficient levels of dopant confinement, these systems behave according to the theoretical framework for EEI in 2D disordered conductors as described by Altshuler and Aronov [24]. Embedded Si:P δ layers confined by a locking layer prior to Si encapsulation exhibit a carrier density dependence of derived charge screening lengths that agree within two standard deviations of uncertainty with expected values calculated based on the Thomas-Fermi approximation to the Lindhard theory, which describes the effects of electric field screening by electrons in a solid [29,30]. Consequently, these embedded Si:P systems may be understood to be 2D disordered metallic systems with 2D EEI. Conversely, embedded Si:P layers not well confined by a locking layer prior to Si overgrowth exhibit signatures of three-dimensional (3D) disordered conducting systems. The correspondence between synthesis and dimensionality of electron transport behavior and EEI described here improves the link between devices in the real world and calculated electronic structures [31] and device simulations [32].

II. METHODS

Sample synthesis followed the methods described previously by Deng *et al.* [33] and detailed in the Supplemental Material [34] (also see [35–41]). Four samples were prepared for this study to investigate the physical nature of charge conduction in embedded Si:P layers at different dopant densities above the metal-insulator transition for P-doped Si:

A1. A sample with a maximally P-doped embedded Si:P δ layer (approximately one-in-four Si replaced by a P atom) produced by saturation dosing a pristine Si (100) surface with PH$_3$ prior to dopant incorporation, followed by the growth of a 15-monolayer (ML) locking layer (LL) grown at room temperature to limit dopant segregation during subsequent processing, and encapsulation by Si overgrowth at 250 °C—the *locking layer saturation* PH$_3$ *dose sample*.

A2. A sample with a medium P-dopant density in the embedded Si:P δ layer confined by a 15-ML locking layer prior to Si encapsulation—the *locking layer medium* PH$_3$ *dose sample*.

A3. A sample with a low P-dopant density (close to the metal-insulator transition for P-doped Si) in the embedded Si:P δ-layer confined by a 15-ML locking layer prior to Si encapsulation—the *locking layer low* PH$_3$ *dose* sample.

B. A sample with a maximally P-doped embedded Si:P δ layer with no locking layer deposited prior to Si encapsulation—the *no locking layer saturation* PH$_3$ *dose sample*.

Analysis of the results of a secondary ion mass spectrometry (SIMS) measurement, following the methodology of Wang *et al.* [42] and discussed in the Supplemental Material [34], reveals approximate thicknesses of the conducting portions of the embedded Si:P layers (Table I). These initial findings are a promising indication that a locking layer confines P to the δ layer. SIMS, however, remains somewhat limited as a means of resolving the thickness of the δ layers in these Si:P samples, [21] motivating us to use a magnetotransport-based method for measuring the thickness of the embedded conducting layer based on a careful analysis of the weak localization signal. We apply a method that Mensz and Wheeler demonstrated has subangstrom sensitivity in measurements of the conducting layer thickness of Si inversion layers in a Si MOSFET, for which they report a value of 0.21 ± 0.015 nm. [43] By using a sensitive magnetotransport-based measurement for conducting layer thickness, we are able to perform a self-contained set of magnetotransport measurements that allow us to directly compare the transport behavior of well-confined embedded Si:P layers grown with a locking layer prior to Si encapsulation (samples A1–A3) and Si:P layers poorly confined due to lack of a locking layer prior to Si encapsulation (sample B). With further analysis of these magnetotransport results, electron-electron scattering parameters can be extracted which give us further insights into dimensionality and transport behavior in these materials.

Electrical measurements were performed on samples etched into a Hall bar geometry with channel lengths of 100 μm and channel widths of 20 μm by using standard lithographic techniques. Samples were affixed to the end of an insert rod and loaded into a continuous closed-cycle cryostat with a superconducting magnet (maximum field of 12 T). With an approximately 1-μA rms ac current applied along the channel and longitudinal and transverse (Hall) voltages measured simultaneously by a lock-in amplifier technique, magnetoresistance measurements were taken at temperatures ranging from a base temperature of 2 K up to 16 K with magnetic fields swept from −5 T to +5 T applied both perpendicular ($\mathbf{B}_\perp$) and parallel ($\mathbf{B}_{||}$) to the planes of the samples. Temperatures were measured by a thermocouple positioned near the sample.

III. RESULTS

We analyze the low-temperature magnetoresistivity data with the magnetic field oriented perpendicular to and parallel

TABLE I. Experimental results for Si:P δ-layer samples measured at base temperature (2 K). Two-dimensional carrier concentration n_{2D}, mobility μ, Fermi wavelength k_F, and mean-free-path length l were extracted from Hall measurement analysis. Phase coherence length l_ϕ was extracted from fits to Eq. (1). Weak-localization-measured thickness Δ was extracted from fits to Eq. (2) and is comparable to the SIMS measured thickness. Uncertainties in l_ϕ and Δ are dominated by the fitting errors (uncertainties in the fundamental parameters effective charge e, carrier mass m, and Fermi wavelength k_F are not included). Uncertainties are given as one-sigma standard deviations. The fitting errors in n_{2D}, μ, k_F, and l are less than 1% of the values.

Sample	$n_{2D}(\text{cm}^{-2})$	$\mu(\text{cm}^2\,\text{V}^{-1}\,\text{s}^{-1})$	$k_F(\text{nm}^{-1})$	l (nm)	l_φ (nm)	Δ (nm)	SIMS-measured Si:P layer thickness (nm)
A1	1.87×10^{14}	42.7	2.4	6.8	97 ± 0.2	1.7 ± 0.01	≈ 7.2
A2	4.57×10^{13}	47.2	1.2	3.7	41.4 ± 0.02	1.3 ± 0.02	≈ 2.2
A3	8.47×10^{12}	42.6	0.5	1.4	12.7 ± 0.03	1.7 ± 0.02	≈ 2.5
B	1.99×10^{14}	79.1	2.5	13	181 ± 0.7	8.8 ± 0.04	≈ 15

to the samples at a range of temperatures based on semiclassical transport theory to derive the values for the 2D carrier concentration n_{2D}, mobility μ, Fermi wavelength k_F, and the mean-free-path length l. The details of this analysis are presented in the Supplemental Material [34] and in previous work [21]. Parameters associated with electrical transport extracted from measurements at base temperature are given in Table I.

We carefully analyze the weak localization (WL) signal $\delta\sigma_{WL}$—the contribution to the conductivity due to the quantum interference of self-intersecting charge carrier scattering paths. This effect leads to an increased probability of localization (increased resistivity) when the phase coherence length of the traveling mode is greater than the total length of the scattering path. In 2D and at zero magnetic field, $\delta\sigma_{WL}(B=0)$ is given by [44]

$$\delta\sigma_{WL}(B=0) = \left(\frac{e^2}{2\pi^2\hbar}\right)\ln\left(\frac{\tau}{\tau_\phi}\right). \tag{1}$$

With a $0\,\text{T} \leqslant |B| \leqslant 1\,\text{T}$ magnetic field applied perpendicular to ($B_\perp$) and parallel to ($B_\parallel$) the sample plane of the samples [Figs. 1(a)–1(d)], the change in conductivity relative to $\delta\sigma_{WL}(B=0)$ for $\delta\sigma_{WL}(B_\perp)$ and $\delta\sigma_{WL}(B_\parallel)$ is given by the following equations [45,46,21]:

$$\delta\sigma_{WL}(B_\perp) - \delta\sigma_{WL}(0) = \left(\frac{e^2}{2\pi^2\hbar}\right)\left[\psi\left(\frac{1}{2} + \frac{\hbar}{4eD\tau_\phi B_\perp}\right)\right.$$
$$\left. - \psi\left(\frac{1}{2} + \frac{\hbar}{4eD\tau B_\perp}\right) - \ln\left(\frac{\tau}{\tau_\phi}\right)\right], \tag{2}$$

$$\delta\sigma_{WL}(B_\parallel) - \delta\sigma_{WL}(0) = \left(\frac{e^2}{2\pi^2\hbar}\right)\ln\left(1 + \sqrt{4\pi}\frac{e^2}{\hbar^2}\frac{l_c}{l}l_\phi^2\Delta^2 B_\parallel\right). \tag{3}$$

Here, $D = \frac{\hbar^2 k_F^2}{2m^2}\tau$ is the diffusion coefficient, τ_ϕ is the dephasing time, $l_\phi = \sqrt{D\,\tau_\phi}$ is the average phase coherence length of the traveling modes, Ψ is the digamma function, $l_c = 1/\sqrt{n_{2D}}$ is the correlation length (a measure of surface roughness roughly equivalent to the mean donor spacing) [31], and Δ is the mean thickness of the conducting layer. The values of l_ϕ and Δ for all four samples measured at base temperature are given in Table I. Dividing the 2D carrier

concentration, n_{2D}, by Δ gives a good measurement of the 3D carrier concentration, n_{3D}, of the embedded Si:P layer. For the Si:P layers of samples A1, A2, A3, and B, we report n_{3D} values at 2 K of 1.1×10^{21}, 3.6×10^{20}, 4.9×10^{19}, and 2.3×10^{20} cm^{-3}, respectively. We calculate approximate Thouless lengths, $l_{TH} \approx \sqrt{l\,l_\phi}$, which represent the effective size scale for quantum interference effects [44], of 26, 12, 4, and 49 nm for Samples A1, A2, A3, and B, respectively. For all samples, $l_{TH} > \Delta$, suggesting that these samples behave appropriately according to weak localization theory for 2D systems.

We perform the weak localization measurement with the magnetic field applied perpendicular to the sample at different temperatures [Fig. 1(b)] and, fitting to Eq. (2), extract l_ϕ at several temperatures between 2 and 16 K, shown in Fig. 1(c) on a log-log plot. Fitting this curve to the power-law equation, shown in Fig. 1(c) with uncertainty given as the one-sigma fitting error, offers insight into the electron-electron scattering behavior in these conducting layers. l_ϕ with a $T^{-1/2}$ temperature dependence is expected for phase-decohering electron-electron scattering in a 2D disordered conducting system. Alternatively, l_ϕ with a $T^{-3/4}$ temperature dependence is expected to arise from large energy transfer electron-electron scattering interactions typically observed in 3D disordered conducting systems. [24] We see that the temperature dependence of l_ϕ in both the saturation (A1) and medium (A2) PH$_3$ dose samples grown with a locking layer is close to the $T^{-1/2}$ temperature dependence expected in 2D disordered conducting systems. Conversely, the temperature dependence of l_ϕ in the saturation PH$_3$ dose sample grown without a locking layer (B) is close to the $T^{-3/4}$ temperature dependence expected in 3D disordered conducting systems. Unlike for the samples with the Si:P confined by a locking layer prior to Si overgrowth (samples A1 and A2), the poor confinement of the Si:P layer in sample B appears to cause electron-electron scattering in this system to behave like a 3D disordered conducting system. This suggests that the dimensionality of the EEI may be different from the dimensionality of the quantum interference effects (e.g., weak localization), as observed for Sample B.

Corrections to the conductivity from EEI that do not involve self-intersecting closed loops provide useful parameters from which to extract information on the screening lengths of the charge carriers involved in conduction in the Si:P δ layers. The following analysis allows us to assess the validity of the assumption that the embedded Si:P systems studied here are
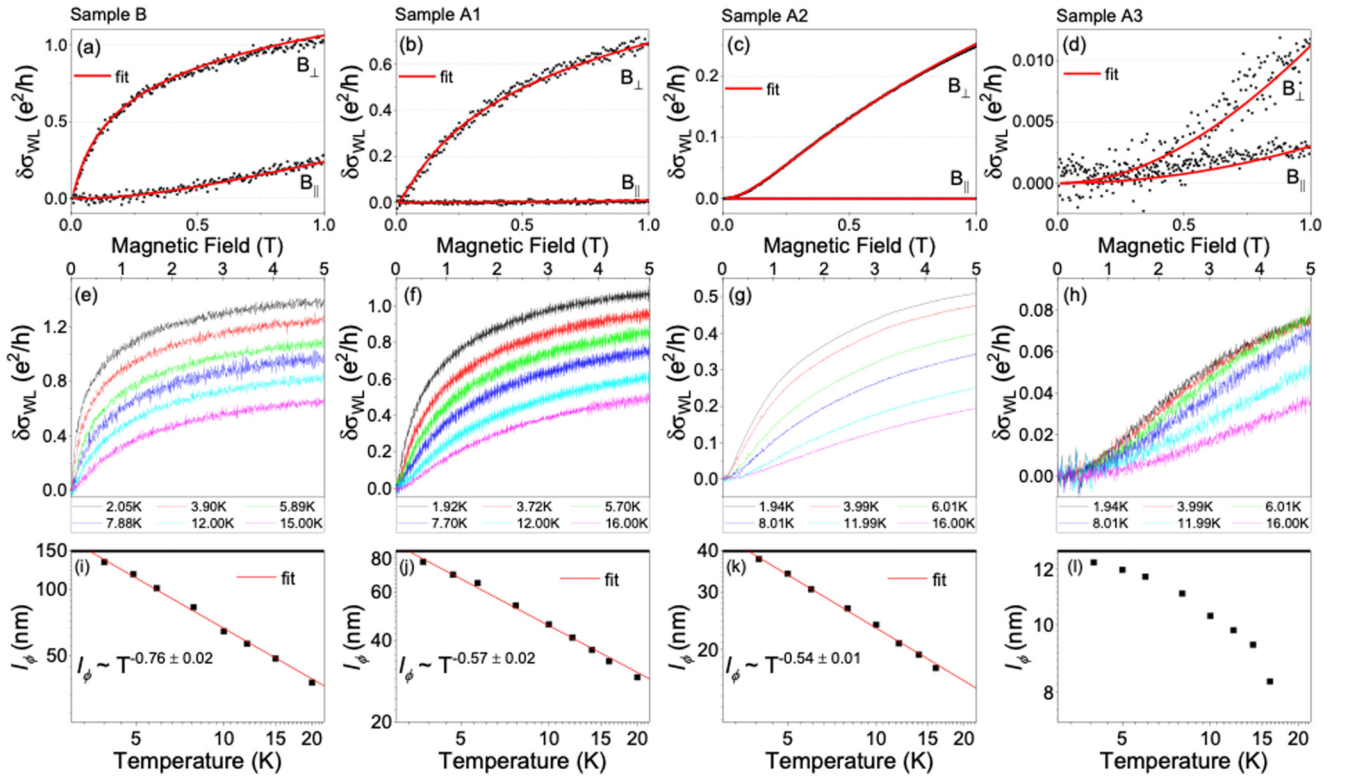
FIG. 1. (a)–(d) Change in conductivity due to quantum interference effects attributed to weak localization as a function of applied magnetic field. Measurements were taken at 2 K with the magnetic field applied normal to the sample plane, $\mathbf{B}_\perp$, and with the magnetic field applied parallel to the sample plane, $\mathbf{B}_\parallel$. Fits to Eqs. (2) and (3) are shown as red lines for all plots. (e)–(h) Conductivity contributions from weak localization as a function of $\mathbf{B}_\perp$ at various temperatures. (i)–(l) Log-log plot of the temperature dependence of the phase coherence length. From left to right: saturation dose PH$_3$ sample with no locking layer, B (a), (e), (i); saturation dose PH$_3$ sample with a locking layer, A1 (b), (f) , (j); medium dose PH$_3$ sample with a locking layer, A2 (c), (g), (k); low-dose PH$_3$ sample with a locking layer, A3 (d), (h), (l).

highly disordered, highly confined 2D conducting systems. We consider a 2D magnetoconductivity tensor that includes a temperature-independent classical Drude conductivity term,

$$\boldsymbol{\sigma_D} = \frac{n\,e\,\mu}{1 + \mu^2\,B^2}\begin{pmatrix} 1 & -\mu\,B \\ \mu\,B & 1 \end{pmatrix}, \qquad (4)$$

and a 2D tensor representing the contribution to the magnetoconductivity from EEI,

$$\boldsymbol{\delta\sigma_{ee}} = \begin{pmatrix} \delta\sigma_{ee} & 0 \\ 0 & \delta\sigma_{ee} \end{pmatrix}, \qquad (5)$$

where EEIs in the diffusion channel do not contribute to the Hall conductivity, $\delta\sigma_{ee,xy} = 0$. This gives the total magnetoconductivity as $\boldsymbol{\sigma} = \boldsymbol{\sigma_D} + \boldsymbol{\delta\sigma_{ee}}$.

At cryogenic temperatures in semiconductors, according to the Bloch-Grüneisen formula [47] electron-electron effects are predicted to have a larger temperature dependence than phonon scattering and other scattering effects. We therefore approximate the classical Drude magnetoconductivity tensor as that which would be measured at absolute zero temperature, with corresponding on-diagonal tensor term and Hall coefficient at absolute zero given by σ_D^0 and R_H^0, respectively. We estimate the value of σ_D^0, defined as $\sigma_D^0 = ne\mu$, as the zero-field conductivity measured at the lowest temperature reached in this study, about 2 K, with the contribution from weak localization, described earlier in this paper, subtracted

out. We likewise estimate the value of R_H^0 as the Hall coefficient measured at the lowest temperature of about 2 K. Altshuler and Aronov [24] demonstrated that EEI contribute to an adjustment to the Hall coefficient, δR_H, given by

$$\frac{\delta R_H}{R_H^0} = -2\frac{\delta\sigma_{ee}}{\sigma_D^0}. \qquad (6)$$

The contribution to conductivity due to EEI can also be approximated from a measurement of $\sigma_{xx}(B)$ at a sufficiently strong magnetic field to suppress weak localization, $B \gg \frac{\hbar}{4eD\tau_\phi}$. In this case $\delta\sigma_{ee}(T) \approx \sigma_{xx}(B \gg \hbar/4eD\tau_\phi, T) - \sigma_{xx}(B \gg \hbar/4eD\tau_\phi, T = 0)$. Here, the subtracted second term is measured at the lowest temperature reached in this study of about 2 K. $\delta\sigma_{ee}$ calculated this way is expected to agree with $\delta\sigma_{ee}$ calculated from Eq. (6) within a factor of 2 [48] and is a useful check. However, larger than factor-of-2 deviations may arise if there are other temperature-dependent scattering and magnetoconductivity effects. $\delta\sigma_{ee}$ calculated by using magnetoconductivities measured at $B = 12$ T agrees with values calculated using Eq. (6) within a factor of close to 1 for samples A1, A2, and B. However, we observe slightly higher deviations between $\delta\sigma_{ee}$ values calculated by these two methods for the sample near the metal-insulator transition, sample A3, approaching a factor of 5 difference at 20 K.

We are more confident in the determination of $\delta\sigma_{ee}$ from the Hall measurements relative to values extracted from mea-

surements of the high-field magnetoconductivity. The measurement of $\delta\sigma_{ee}$ from $\sigma_{xx}(B)$ at high fields is based upon the presumption that only contributions from EEI remain when the magnetic field is raised high enough to suppress weak localization. In practice, it requires identifying an appropriate magnetic field, $B \gg \hbar/4eD\tau_\phi$, and accounting for the temperature dependence of additional interactions such as the temperature- and magnetic-field-dependent $\delta\sigma_{ee}(B, T)$ contribution from spin splitting in the particle-hole diffusion channel and temperature-dependent coupling in the particle-particle diffusion channel [44]. Choosing a sufficiently high field at which to measure $\delta\sigma_{ee}$ is further complicated in highly disordered systems, such as these Si:P δ layers, by a weak localization feature that is quite wide, often contributing to a positive magnetoconductance over more than 1 T. These complications are illustrated in the analysis of sample A3, which is near the metal-insulator transition. It is expected to support temperature-dependent interaction mechanisms that impact the magnetoconductivity in addition to WL and EEI, leading to the disagreement in $\delta\sigma_{ee}$ extracted by the two approaches. Determining $\delta\sigma_{ee}$ from the slope of the Hall curve according to Eq. (6), on the other hand, permits the measurement of the $\ln(T)$-dependent $\delta\sigma_{ee}$ term directly [49], and has been confirmed experimentally [48,50]. Furthermore, determining the electron-electron contribution to the conductivity from Hall measurements leads to a smaller uncertainty of the measurement, even when including the fitting error. Consequently, we use the values of $\delta\sigma_{ee}$ calculated from Eq. (6) in the remainder of our analysis of EEI in these samples.

In this system, a highly disordered conducting system at low temperature in the diffusive charge transport regime where $\frac{kT\tau}{\hbar} \ll 1$, we expect $\delta\sigma_{ee}$, and therefore δR_H, to have a logarithmic temperature dependence [51] given by

$$\delta\sigma_{ee}(T) = g\frac{e^2}{2\pi^2\hbar}\ln\left(\frac{kT\tau}{\hbar}\right) \tag{7a}$$

$$= g\frac{e^2}{2\pi^2\hbar}\ln(T) + g\frac{e^2}{2\pi^2\hbar}\ln\left(\frac{k\tau}{\hbar}\right), \tag{7b}$$

where the factor g depends on the Fermi wavelength and the screening length, and the term on the right in Eq. (7b) is a constant. We measure the contribution to the conductivity from EEI, $\delta\sigma_{ee}$, at various temperatures by extracting its value from the Hall coefficient measured at these temperatures. Inverting the conductivity tensor, $\boldsymbol{\sigma}$, for $\delta\sigma_{ee} \ll ne\mu$ and $\mu B \ll 1$, we get an approximate resistivity tensor, $\boldsymbol{\rho}$, of

$$\boldsymbol{\rho} \approx \frac{1}{ne\mu}\begin{pmatrix} 1 & -\mu B \\ \mu B & 1 \end{pmatrix}$$
$$- \frac{\Delta\sigma_{ee}}{(ne\mu)^2}\begin{pmatrix} 1-\mu^2 B^2 & -2\mu B \\ 2\mu B & 1-\mu^2 B^2 \end{pmatrix}, \tag{8}$$

from which we obtain a value for the transverse resistivity, ρ_{xy}, that corresponds with Eq. (3):

$$\rho_{xy} = -\frac{1}{ne}\left(1 - \frac{2\,\delta\sigma_{ee}}{ne\mu}\right)B = R_H^0\left(1 - 2\frac{\delta\sigma_{ee}}{\sigma_D^0}\right)B. \tag{9}$$

From this, the Hall resistivity at each temperature is given as $R_H(T) = R_H^0[1 - 2\frac{\delta\sigma_{ee}(T)}{\sigma_D^0}]$, from which $\delta\sigma_{ee}(T)$ can be
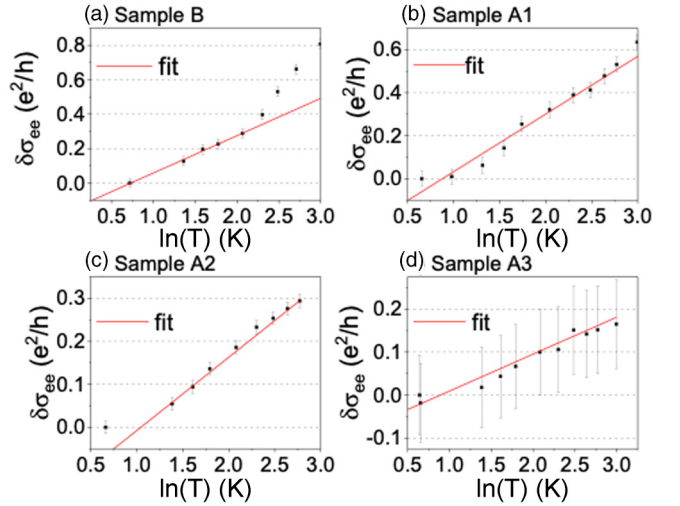
FIG. 2. The contribution to the conductivity from electron-electron interactions as a function of the natural log of the temperature. The linear fit to the data gives an approximate value for the factor g in Eqs. (7a) and (7b). Error bars show the total error calculated from statistical and fitting errors.

extracted. $\delta\sigma_{ee}$ is plotted as a function of $\ln(T)$ and fitted to Eq. (7b) (Fig. 2), the linear slope of which provides the parameter g. Note that for sample B, there appears to be a kink in the curve at about 8 K. An explanation for this is beyond the scope of this study. However, it appears that this poorly confined δ-layer sample does not behave according to the predictive models for highly disordered 2D diffusively conducting systems at low temperature. In spite of this, we use the portion of the data that is linear with $\ln(T)$ at the lower temperatures, where the system is more ideally in the highly disordered, diffusive transport regime of $\frac{kT\tau}{\hbar} \ll 1$, for our fit to obtain g for this sample.

For the diffusive correction to the conductivity due to EEI in a highly disordered 2D system at low temperature, $g = 1 + \frac{3}{4}\lambda_\sigma^{(j=1)}$, where $\lambda_\sigma^{(j=1)}$ is a dimensionless electron-electron exchange correction for two interacting spin-$\frac{1}{2}$ electrons [24]. $\lambda_\sigma^{(j=1)}$ can be expressed in terms of a Hartree term, F, as

$$\lambda_\sigma^{(j=1)} = 4\left[1 - 2\frac{\left(1 + \frac{1}{2}F\right)\ln\left(1 + \frac{1}{2}F\right)}{F}\right]. \tag{10}$$

In the purely 2D case, the Hartree term is given by

$$F = \frac{1}{\pi(x^2-1)^{1/2}}\ln\left[\frac{x+(x^2-1)^{1/2}}{x-(x^2-1)^{1/2}}\right], \quad x = \frac{2k_F}{\kappa_{TF}}, \tag{11}$$

where k_F is the Fermi wave number shown in Table I. Note that in our analysis, we excluded the higher-order terms to the correction to conductivity calculated by Zala et al. [52], which extend the corrections to conductivity due to EEI beyond the low-temperature diffusive regime. However, these terms may prove useful in future studies on these systems.

Solving Eq. (11) gives the Thomas-Fermi wave vector, κ_{TF}, the inverse of which is the Thomas-Fermi screening length, l_{TF}. The Thomas-Fermi screening length is computed for all four samples and plotted versus the 3D carrier con-
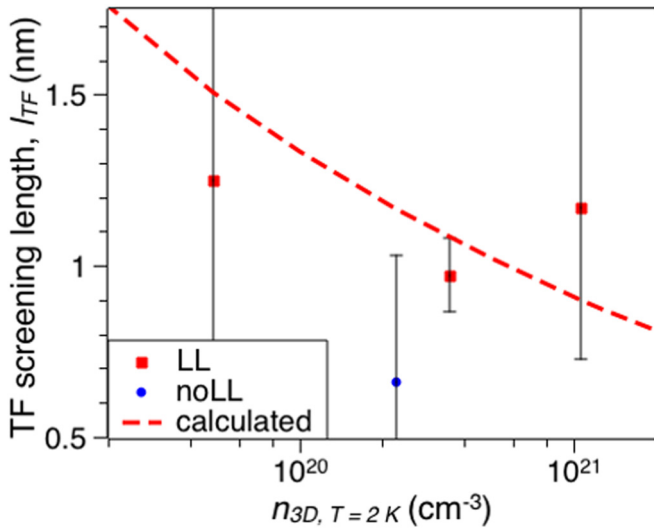
FIG. 3. Thomas-Fermi screening length, l_{TF} as a function of 3D carrier concentration for the three locking layer samples A1, A2, and A3 (LL) and no locking layer sample B (noLL). The l_{TF} values computed from theory [Eq. (12)] are shown as a red dashed line. Error bars show two standard deviations from the total error calculated from statistical and fitting errors.

centration values calculated in the previous section of this manuscript in Fig. 3. The measured l_{TF} values for the samples grown with a locking layer (samples A1–A3) show good agreement—within two standard deviations—with the calculated Thomas-Fermi screening length, which is given by

$$l_{\text{TF}} = \left[\frac{m^* \, e^2}{\pi \, \varepsilon \, \hbar^2} \left(\frac{3 \, n_{3\text{D}}}{\pi} \right)^{1/3} \right]^{-1/2}, \qquad (12)$$

and is included in Fig. 3 as a dashed red line. The measured l_{TF} value in the sample with no locking layer (B) shows a larger discrepancy of greater than two standard deviations from the calculated l_{TF} value. This is an unsurprising result for this sample, with its poorly confined Si:P system and approximately $T^{-3/4}$ temperature dependence of l_ϕ, in which we predict EEI behavior expected for a 3D disordered conductor, not a 2D disordered conductor for which the Aronov and Altschuler theoretical framework is appropriate. Moreover, an *a priori* presumed effect of dopant confinement on screening lengths would be that suppression of screening lengths would be more likely to be observed for dimensionally confined systems, such as those in the locking layer samples, than for the poorly confined no locking layer system. The reason for this is that out-of-plane electric fields are not contributing to any consequential screening when the conducting charges are confined to two dimensions. That we instead measure the greatest suppression of screening length relative to the expected value for Sample B further indicates that, for the purposes of our EEI analysis, the assumption of tight confinement of the dopants and a 2D nature of the conducting system are not valid in this sample.

IV. CONCLUSION

In summary, we used a self-contained magnetotransport investigation to study low-temperature charge carrier transport physics and quantify screening lengths for embedded Si:P δ layers. We show that, for systems well confined by a locking layer, these systems behave according to Altschuler and Aronov's framework for disordered 2D conducting systems. From our calculations, we derive charge screening lengths for the locking layer systems that well match those predicted from the Thomas-Fermi theory. The no locking layer Si:P system, with poorly confined dopants, does not appear to behave according to this model for 2D systems, and instead expresses a temperature dependence of the phase coherence related to electron-electron interaction physics expected in 3D disordered conducting systems. As part of the suite of measurements and analysis that lead to this result, analysis of the weak localization signal, described in detail in this paper, demonstrates its promise as an accurate method of measuring the δ-layer thickness. Overall, this work shows that it is appropriate to treat embedded Si:P δ layers confined by a locking layer as 2D disordered metallic systems with 2D EEIs for the purpose of designing and modeling embedded P dopant-based Si quantum computing devices.

[1] J. Lyding, T. C. Shen, J. Hubacek, J. Tucker, and G. Abeln, Nanoscale patterning and oxidation of H-passivated Si (100)- 2 × 1 surfaces with an ultrahigh vacuum scanning tunneling microscope, Appl. Phys. Lett. **64**, 2010 (1994).

[2] D. K. Ferry, Ohm's law in a quantum world, Science **335**, 45 (2012).

[3] S. Schofield, N. Curson, M. Simmons, F. Rueß, T. Hallam, L. Oberbeck, and R. Clark, Atomically Precise Placement of Single Dopants in Si, Phys. Rev. Lett. **91**, 136104 (2003).

[4] A. Fuhrer, M. Füchsle, T. Reusch, B. Weber, and M. Simmons, Atomic-scale, all epitaxial in-plane gated donor quantum dot in silicon, Nano Lett. **9**, 707 (2009).

[5] J. Wyrick, X. Wang, R. V. Kashid, P. Namboodiri, S. W. Schmucker, J. A. Hagmann, K. Liu, M. D. Stewart, Jr., C. A. Richter, G. W. Bryant, and R. M. Silver, Atom-by-atom fabrication of single and few dopant quantum devices, Adv. Funct. Mater. **29**, 1903475 (2019).

[6] B. Weber, S. Mahapatra, H. Ryu, S. Lee, A. Fuhrer, T. Reusch, D. Thompson, W. Lee, G. Klimeck, and L. C. Hollenberg, Ohm's law survives to the atomic scale, Science **335**, 64 (2012).

[7] S. McKibbin, G. Scappucci, W. Pok, and M. Simmons, Epitaxial top-gated atomic-scale silicon wire in a three-dimensional architecture, Nanotechnology **24**, 045303 (2013).

[8] M. Füchsle, S. Mahapatra, F. Zwanenburg, M. Friesen, M. Eriksson, and M. Y. Simmons, Spectroscopy of few-electron single-crystal silicon quantum dots, Nat. Nanotechnol. **5**, 502 (2010).

[9] E. Bussmann, M. Rudolph, G. Subramania, S. Misra, S. Carr, E. Langlois, J. Dominguez, T. Pluym, M. Lilly, and M. Carroll, Scanning capacitance microscopy registration of buried atomic-precision donor devices, Nanotechnology **26**, 085701 (2015).

[10] M. Füchsle, J. A. Miwa, S. Mahapatra, H. Ryu, S. Lee, O. Warschkow, L. C. Hollenberg, G. Klimeck, and M. Y. Simmons, A single-atom transistor, Nat. Nanotechnol. **7**, 242 (2012).

[11] B. E. Kane, A silicon-based nuclear spin quantum computer, Nature **393**, 133 (2012).

[12] F. A. Zwanenburg, A. S. Dzurak, A. Morello, M. Y. Simmons, L. C. Hollenberg, G. Klimeck, S. Rogge, S. N. Coppersmith, and M. A. Eriksson, Silicon quantum electronics, Rev. Mod. Phys. **85**, 961 (2013).

[13] C. D. Hill, E. Peretz, S. K. Hile, M. G. House, M. Füchsle, S. Rogge, M. Y. Simmons, and L. C. Hollenberg, A surface code quantum computer in silicon, Sci. Adv. **1**, e1500707 (2015).

[14] S. Roy and A. Asenov, Where do the dopants go? Science **309**, 388 (2005).

[15] H. J. Gossman, E. Schubert, D. Eaglesham, and M. Cerullo, Low-temperature Si molecular beam epitaxy: Solution to the doping problem, Appl. Phys. Lett. **57**, 2440 (1990).

[16] D. Eaglesham, Semiconductor molecular beam epitaxy at low temperatures, J. Appl. Phys. **77**, 3597 (1995).

[17] S. McKibbin, W. Clarke, A. Fuhrer, T. Reusch, and M. Y. Simmons, Investigating the regrowth surface of Si:P δ-layers toward vertically stacked three dimensional devices, Appl. Phys. Lett. **95**, 233111 (2009).

[18] L. Oberbeck, N. Curson, M. Simmons, R. Brenner, A. Hamilton, S. Schofield, and R. Clark, Encapsulation of phosphorus dopants in silicon for the fabrication of a quantum computer, Appl. Phys. Lett. **81**, 3197 (2002).

[19] K. Goh, L. Oberbeck, M. Y. Simmons, A. Hamilton, and R. Clark, Effect of encapsulation temperature on Si:P δ-doped layers, Appl. Phys. Lett. **85**, 4953 (2004).

[20] J. G. Keizer, S. Koelling, P. M. Koenraad, and M. Y. Simmons, Suppressing segregation in highly phosphorus doped silicon monolayers, ACS Nano **9**, 12537 (2015).

[21] J. A. Hagmann, X. Wang, P. Namboodiri, J. Wyrick, R. Murray, M. D. Stewart, Jr., R. M. Silver, and C. A. Richter, High resolution thickness measurements of ultrathin Si:P monolayers using weak localization, Appl. Phys. Lett. **112**, 043102 (2018).

[22] E. J. Kramer, Depth profiling methods that provide information complementary to neutron reflectivity, Physica B (Amsterdam, Neth.) **173**, 189 (1991).

[23] Y. Homma, H. Takenaka, F. Toujou, A. Takano, S. Hayashi, and R. Shimizu, Evaluation of the sputtering rate variation in SIMS ultra-shallow depth profiling using multiple short-period delta layers, Surf. Interface Anal. **35**, 544 (2003).

[24] B. L. Altshuler and A. G. Aronov, Electron-electron interaction in disordered conductors, in *Electron-Electron Interaction in Disordered Systems*, edited by A. L. Efros and M. Pollak (Elsevier Science Publishing Company, New York, 1985).

[25] L. Petit, H. G. J. Eenick, M. Russ, W. I. L. Lawrie, N. W. Hendrickx, S. G. J. Philips, J. S. Clarke, L. M. K. Vandersypen, and M. Veldhorst, Universal quantum logic in hot silicon qubits, Nature **580**, 355 (2020).

[26] C. H. Yang, R. C. C. Leon, J. C. Hwang, A. Saraiva, T. Tanttu, W. Hwang, J. Camirand Lemyre, K. W. Chan, K. Y. Tan, F. E. Hudson, K. M. Itoh, A. Morello, M. Pioro-Ladrière, A. Laucht, and A. S. Dzurak, Operation of a silicon quantum processor unit cell above one kelvin, Nature **580**, 350 (2020).

[27] A. Y. Kuntsevich, L. A. Morgun, and V. M. Pudalov, Electron-electron interaction correction and magnetoresistance in tilted fields in Si-based two-dimensional systems, Phys. Rev. B **87**, 205406 (2013).

[28] G. M. Minkov, O. E. Rut, A. V. Germanenko, A. A. Sherstobitov, V. I. Shashkin, O. I. Khrykin, and V. M. Daniltsev, Quantum corrections to the conductivity in two-dimensional systems: Agreement between theory and experiment, Phys. Rev. B **64**, 235327 (2001).

[29] J. Lindhard, On the properties of a gas of charged particles, K. Dan. Vidensk. Selsk. Mat. Fys. Medd. **28**, 8 (1954).

[30] N. W. Ashcroft and N. D. Mermin, *Solid State Physics* (Thomson Learning, Toronto, 1976).

[31] S. Lee, H. Ryu, H. Campbell, L. C. L. Hollenberg, M. Y. Simmons, and G. Klimeck, Electronic structure of realistically extended atomistically resolved disordered Si:P δ-doped layers, Phys. Rev. B **84**, 205309 (2011).

[32] G. Klimeck, R. Lake, R. C. Bowen, W. R. Frensley, and T. S. Moise, Quantum device simulation with a generalized tunneling formula, Appl. Phys. Lett. **67**, 2539 (1995).

[33] X. Deng, P. Namboodiri, K. Li, X. Wang, G. Stan, A. F. Myers, X. Cheng, T. Li, and R. M. Silver, Silicon epitaxy on H-terminated Si (100) surfaces at 250 °C, Appl. Surf. Sci. **378**, 301 (2016).

[34] See Supplemental Material at http://link.aps.org/supplemental/10.1103/PhysRevB.101.245419 for sample synthesis details, details on the SIMS measurement and analytical methodologies, and details on the magnetotransport analysis.

[35] J. G. Keizer, S. R. McKibbin, and M. Y. Simmons, The impact of dopant segregation on the maximum carrier density in Si:P multilayers, ACS Nano **9**, 7080 (2015).

[36] M. Juhel, F. Laugier, D. Delille, C. Wyon, L. F. T. Kwakman, and M. Hopstaken, SIMS depth profiling of boron ultra shallow junctions using oblique O2+ beams down to 150 eV, Appl. Surf. Sci. **252**, 7211 (2006).

[37] W. Vandervorst, Semiconductor profiling with sub-nm resolution: Challenges and solutions, Appl. Surf. Sci. **255**, 805 (2008).

[38] A. Merkulov, P. Peres, S. Choi, F. Horreard, H. U. Ehrke, N. Loibl, and M. Schuhmacher, Advanced secondary ion mass spectroscopy quantification in the first few nanometer of B, P, and As ultrashallow implants, J. Vac. Sci. Technol. B **28**, C1C48 (2010).

[39] T. Ando, A. B. Fowler, and F. Stern, Electronic properties of two-dimensional systems, Rev. Mod. Phys. **54**, 437 (1982).

[40] J. A. Miwa, O. Warschkow, D. J. Carter, N. A. Marks, F. Mazzola, M. Y. Simmons, and J. W. Wells, Valley splitting in a silicon quantum device platform, Nano Lett. **14**, 1515 (2014).

[41] R. Duffy, V. C. Venezia, J. Loo, M. J. P. Hopstaken, M. A. Verheijen, J. G. M. van Berkum, G. C. J. Maas, Y. Tamminga, T. Dao, and C. Demeurisse, Low-temperature diffusion of high-concentration phosphorus in silicon, a preferential movement toward the surface, Appl. Phys. Lett. **86**, 081917 (2005).

[42] X. Wang, J. A. Hagmann, P. Namboodiri, J. Wyrick, K. Li, R. E. Murray, A. Myers, F. Misenkosen, M. D. Stewart, Jr., C. A.

Richter, and R. M. Silver, Quantifying atom-scale dopant movement and electrical activation in Si:P monolayers, Nanoscale **10**, 4488 (2018).

[43] P. M. Mensz and R. G. Wheeler, Magnetoconductance due to parallel magnetic fields in silicon inversion layers, Phys. Rev. B **35**, 2844 (1987).

[44] P. A. Lee and T. V. Ramakrishnan, Disordered electronic systems, Rev. Mod. Phys. **57**, 287 (1985).

[45] S. Hikami, A. I. Larkin, and Y. Nagaoka, Spin-orbit interaction and magnetoresistance in the two dimensional random system, Prog. Theor. Phys. Lett. **63**, 707 (1980).

[46] H. Mathur and H. U. Baranger, Random Berry phase magnetoresistance as a probe of interface roughness in Si MOSFETs, Phys. Rev. B **64**, 235325 (2001).

[47] E. Grüneisen, The dependance of electrical reaction of pure metals on temperature, Ann. Phys. **16**, 530 (1933).

[48] M. J. Uren, R. A. Davies, and M. Pepper, The observation of interaction and localisation effects in a two-dimensional electron gas at low temperatures, J. Phys. C **13**, L985 (1980).

[49] B. L. Altshuler, D. Khmel'nitzkii, A. I. Larkin, and P. A. Lee, Magnetoresistance and Hall effect in a disordered two-dimensional electron gas, Phys. Rev. B **22**, 5142 (1980).

[50] D. J. Bishop, D. C. Tsui, and R. C. Dynes, Nonmetallic Conduction in Electron Inversion Layers at Low Temperatures, Phys. Rev. Lett. **44**, 1153 (1980).

[51] S. Datta, *Electronic Transport in Mesoscopic Systems* (Cambridge University Press, Cambridge, 1995).

[52] G. Zala, B. N. Narozhny, and I. L. Aleiner, Interaction corrections at intermediate temperatures: Longitudinal conductivity and kinetic equation, Phys. Rev. B, **64**, 214204 (2001).